Journal of Nuclear Materials xxx (xxxx) 151941

Contents lists available at ScienceDirect

Journal of Nuclear Materials

journal homepage: http://ees.elsevier.com

Alloying effects on low–energy recoil events in concentrated solid–solution alloys

Shijun Zhao [a,b,*], Bin Liu [c], German D. Samolyuk [a], Yanwen Zhang [a,d], William J. Weber [a,d]

[a] Materials Science and Technology Division, Oak Ridge National Laboratory, Oak Ridge, TN, 37831, USA
[b] Department of Mechanical Engineering, City University of Hong Kong, Hong Kong, China
[c] School of Materials Science and Engineering, Shanghai University, 99 Shanghai, Shanghai, 20044, China
[d] Department of Materials Science and Engineering, University of Tennessee, Knoxville, TN, 37996, USA

ARTICLE INFO

Article history:
Received 24 June 2019
Received in revised form 29 November 2019
Accepted 3 December 2019
Available online xxx

Keywords
Low-energy recoil events
ab initio molecular dynamics
Threshold displacement energy
Concentration solid solution alloys

ABSTRACT

Alloying elements at low-concentrations into pure metals is usually adopted to improve their mechanical properties and irradiation performance. Recently developed single-phase concentrated solid-solution alloys (CSAs) comprised of two or more elements, all at high concentrations, have demonstrated good radiation resistance. CSAs are characterized by their extreme disordered states that arise from the random arrangement of different elements and accompanied random local lattice distortions. In this work, we investigate low-energy recoil events in $Ni_{50}X_{50}$ (X = Fe and Co) CSAs and $Ni_{80}X_{20}$ (X = Fe, Co, Cr, and Pd) CSAs using *ab initio* molecular dynamics simulations to understand the effects of different disorder on defect production in CSAs. The threshold displacement energies are determined along three high-symmetric directions by randomly choosing independent primary knock-on atoms in each direction. As expected, the threshold energies in Ni and its CSAs are anisotropic, with the highest values found in the [111] direction. The calculated threshold energies of Fe in NiFe are smaller than those in NiCo and Ni, especially along the [111] direction. An inspection of the atomic trajectories inside the collision cascade reveals that the effect of chemical disorder outweighs the site-to-site lattice distortions in determining the threshold energies. Especially, different interaction properties between elements due to their different electronic structures are responsible for the observed different threshold energies. The local environment dependence of threshold energies suggests that local elemental arrangement can be used to understand and predict threshold energies in disordered alloys.

1. Introduction

Structural materials for nuclear applications need to endure the harsh environment of high temperatures, high irradiation, and extreme corrosions. Recently developed concentrated solid–solution alloys (CSAs) with two or more principal elements situated in a simple face-centered cubic (*fcc*) or body-centered cubic (*bcc*) lattice have demonstrated exceptional mechanical properties and irradiation resistance [1–5], which make them promising candidate materials in future nuclear reactors. One of the most intriguing properties of these alloys is that their compositions can be tuned widely among different elemental species and concentrations, and thereby, their properties can be tailored accordingly. Therefore, a fundamental understanding of the link between the properties of CSAs and their compositions is of paramount importance for practical applications.

In CSAs, the extreme chemical disorder induced by the random arrangement of different elements changes significantly the defect energy landscape and defect dynamics [4–6]. Specifically, a rougher energy landscape is found in CSAs compared to that in pure metals, which helps to slow down defect diffusion and suppress defect cluster growth [7–9]. While smaller defect clusters in CSAs are readily appreciated both in experimental observations and atomistic simulations [5,10], the initial stage of damage accumulation in CSAs and pure metals shows little difference or even a reversed trend. For example, there are more defects produced in NiFe and NiCoCr than in pure Ni when the damage is less than 0.07 displacement per atom (dpa) [10]. These results call for the examination of damage production mechanisms in CSAs at the very early stage.

It is well established that the defect production and microstructure evolution play key roles in governing the irradiation tolerance of materials [11]. Thus, the knowledge of defect creation mechanism is very important for understanding damage processes and further designing radiation-resistant structural materials. In the damage production stage, one of the basic parameters controlling radiation damage is the threshold displacement energy (E_d), which is the minimum kinetic energy required to permanently displace an atom from its lattice site. The value of E_d may be used to estimate the number of defects created using the Kinchin–Pease (or NRT) equation [12]. It is also a necessary input to calculate the dpa value in irradiated materials based on the SRIM code. Therefore, the full knowledge of E_d and accompanying low-energy re-

* Corresponding author. Materials Science and Technology Division, Oak Ridge National Laboratory, Oak Ridge, TN, 37831, USA.
E-mail address: shijzhao@cityu.edu.hk (S. Zhao)

https://doi.org/10.1016/j.jnucmat.2019.151941
0022-3115/

coil events, including defect production dynamics and defect structures, are essential to evaluate the radiation performance of materials.

Previous studies on defect production have generally focused on pure metals and dilute alloys. For example, the defect structures and values of E_d in dilute Ni–Al alloys with no more than 30% Al content have been investigated in both experiments and molecular dynamics (MD) simulations [13,14]. The results of such studies suggest that alloying with Al has little effect on the E_d values of Ni and Al in NiAl. In CSAs that contain multiple principal elements, defect evolution is expected to be greatly influenced by the complexity of the underlying compositionally–disordered state [15]. Until now, the importance of this disorder in low-energy recoil events has not been explored. Although classical MD (CMD) simulations based on empirical potentials have been used to study defect evolution at an atomic level, their results are dependent on the nature of the employed empirical potentials. Specifically, different potentials result in different conclusions about defect production and defect structures [16]. On the other hand, *ab initio* calculations can describe interatomic interactions through quantum mechanical calculations with the help of density functional theory (DFT). Based on DFT, *ab initio* molecular dynamics (AIMD) has become an important tool to study low-energy recoil events with an *ab initio* accuracy [17,18]. For disordered alloys, there are still no reports about the low-energy recoil events and threshold energies, possibly due to the high computational cost of AIMD.

In this study, we investigate the low-energy recoil events in $Ni_{50}X_{50}$ (X = Fe and Co) and $Ni_{80}X_{20}$ (X = Fe, Co, Cr, and Pd) CSAs, as well as in pure Ni, by AIMD. We consider the disordered states in CSAs by constructing special quasirandom structures (SQS), and the displacement fluctuation is included by equilibrating the structures before the recoil event is initiated. The value of E_d is determined in three high-symmetric directions by randomly choosing independent primary knock-on atoms (PKA) for each atom type, and the resulted defect structures are analyzed. To understand the difference of E_d values in different CSAs, we have made a detailed electronic structure analysis for alloys with different X concentrations from dilute to concentrated regime. We show that electronic properties of different elements are dominant factors in governing atomic interactions and the E_d values.

2. Methods

First-principles calculations were carried out based on DFT as implemented in the Vienna *ab initio* simulation package (VASP) code [19]. Electron-ion interactions were treated within the projector-augmented-wave method [20]. A gradient corrected functional in the Perdew-Burke-Ernzerhof (PBE) form was used to describe the exchange and correlation interactions [21]. The energy cutoff for the plane-wave basis set was set to be 270 eV. Only the Γ point was used during the dynamic simulations. All calculations were performed with spin-polarization to account for the magnetic properties of considered alloys; the magnetic moments of each element were initiated by the results from previous static calculations [15]. The CSAs were modeled by SQS that was constructed by optimization of the Warren-Cowley short range order (SRO) parameters [22,23] through a simulated Monte-Carlo algorithm [15]. In this study, standard PAW potentials without semi-core 3*p* electrons were used.

The recoil event was initiated by assigning certain kinetic energy (E_i) along a specific direction to a selected atom (i.e., PKA). Three high-symmetric directions in the *fcc* lattice were studied, namely [100], [110] and [111] directions. Two different SQS sizes were used depending on the direction of PKA, as was done in a previous study [24]. Specifically, a 6 × 3 × 3 supercell was used for the [100] direction recoils and a 4 × 4 × 4 supercell was employed for all other directions. The structures were first equilibrated at 300 K for 2 ps using the NVT ensemble by controlling the temperature with the Nosé-Hoover thermostat [25,26]. After that, low energy recoil events were simulated using NVE ensembles by keeping the atom number, volume and energy constant. Both the chemical disorder and site-to-site lattice distortions in CSAs were included in this simulation setup. A timestep of 1 fs was used, and the final defect structures were analyzed after 2 ps dynamics runs. Further increasing the simulation time did not result in significant changes in the defect structures [24]. We have made tests with a smaller timestep of 0.5 fs, and no significant changes were found in the trajectories of the PKA. In fact, with a step of 1 fs, the maximal displacement during the recoil event initiated by a 50 eV Ni PKA is around 0.12 Å. Besides, this maximal displacement only occurs at the very beginning of the recoil process. Afterward, the kinetic energy of the PKA decreases rapidly, and the system starts to evolve toward the equilibrium state, in which phase the influence of timestep is small. The same timestep has been used in a number of low-energy recoil simulations based on AIMD [24,27]. The value of E_d was determined by increasing E_i until a stable defect is formed. The uncertainty of E_d was narrowed to 1 eV by setting the energy increment to 1 eV [24,28,29]. The same DFT methodology has been extensively used to calculate E_d values and study low-energy recoil events in different materials [24,27–29].

3. Result

3.1. Equiatomic NiCo and NiFe CSAs

3.1.1. Threshold displacement energies

While the chemical disorder is considered in a similar way for both NiCo and NiFe using SQS supercells, the lattice distortions in NiFe are larger than those in NiCo due to the large atomic size difference between Fe and Ni. To illustrate this effect, the distribution of radial displacement for each atom in Ni, NiCo and NiFe averaged from the last 200 steps within a 2 ps AIMD simulations at 300 K are presented in Fig. 1. Here the radial displacement is measured with respect to a perfect *fcc* lattice. It is clear that the lattice distortions are more pronounced in NiFe compared to NiCo and Ni. This conclusion is in

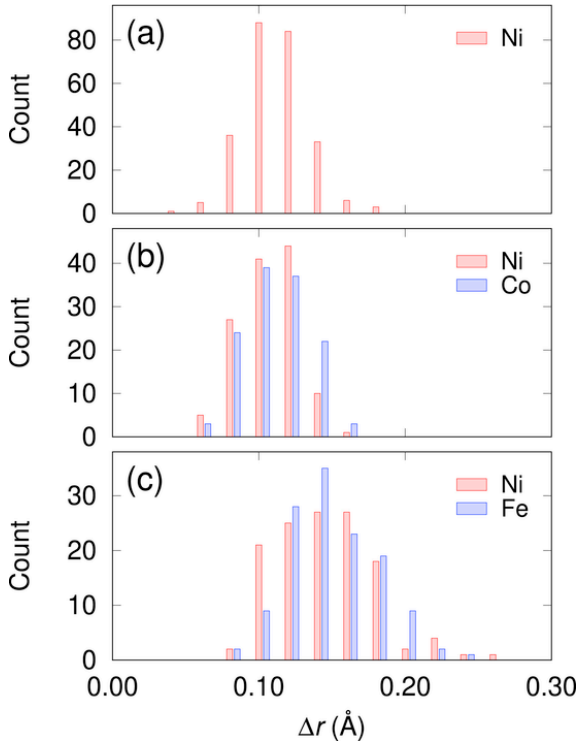

Fig. 1. The distribution of radial displacement with respect to a perfect *fcc* lattice in Ni (a), NiCo (b) and NiFe (c) after 2 ps AIMD simulations at 300 K.

good agreement with our previous displacement results collected from fully optimized SQS structures at 0 K [15]. At the final state, the averaged displacement is 0.11 Å for Ni in pure Ni, 0.11 and 0.12 Å for Ni and Co in NiCo respectively, and 0.15 and 0.16 Å for Ni and Fe in NiFe respectively. These atomic displacements have significant influence on E_d, as will be discussed below.

Because of the random displacement and thermal vibrations, the determined threshold energies are different even for the same PKA type in the same recoil direction. In order to obtain general conclusions on the values of E_d, three atoms are randomly chosen as PKAs for each atom type in each direction, except for Ni and Fe in NiFe along the [111] direction; five independent low-energy recoil events are simulated since we find E_d values are smaller in this direction. All the calculated E_d are summarized in Fig. 2, together with previous results obtained in Ni and ordered NiCo [24].

Fig. 2 shows that E_d values in Ni as well as its CSAs determined by AIMD at 300 K are anisotropic. In particular, E_d values along the [110] direction are the lowest among the three PKA directions considered, whereas E_d values in the [111] direction are the highest. These results are in agreement with previous calculations [24]. It is understandable that large E_d values are observed in the [111] direction since the PKA must surmount large barriers to pass through the triangular centers

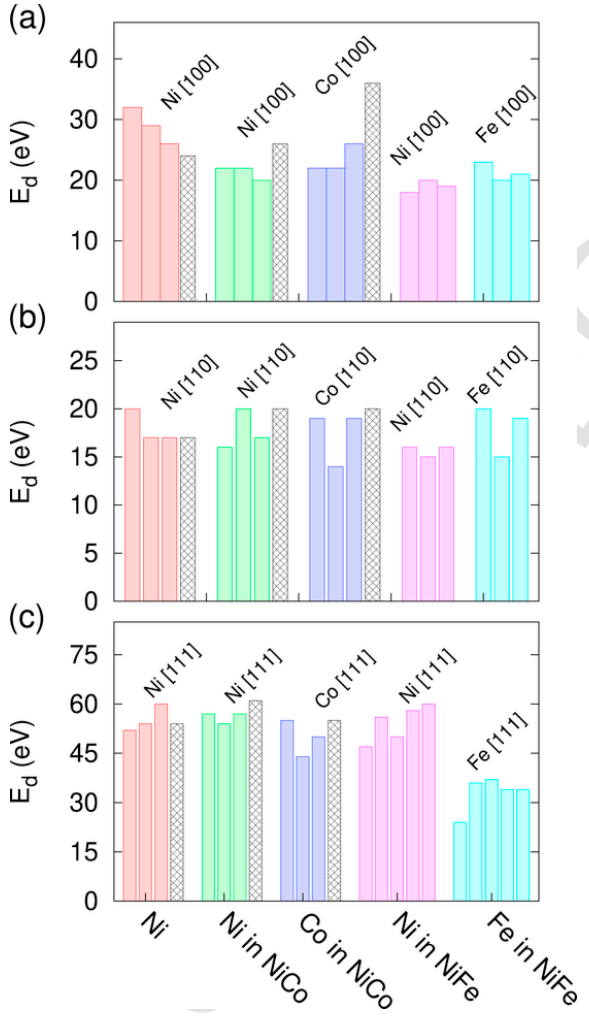

Fig. 2. Threshold displacement energies in pure Ni, NiCo and NiFe determined by three randomly chosen PKA for each atom type: (a) [100] direction, (b) [110] direction and (c) [111] direction. Previous results [24] in Ni and NiCo are shown in black. For Ni and Fe in NiFe along the [111] direction, two additional calculations are performed to confirm the trend of E_d. Note that the E_d value along the [110] direction is defined as the minimal energy required for the PKA to leave its original location.

in adjacent closed-packed {111} planes (ABCABC stacking in *fcc* structures). In the close-packed [110] direction, the recoil leads to a replacement collision sequence that extends to around 30 atoms in length according to our tests using MD simulations with the Bonny potential [30]. To fully include this replacement sequence would require a large supercell containing at least 2700 atoms (a 15 × 15 × 3 supercell). This is not feasible within AIMD simulations. As a result, the value of E_d in this direction is determined by the minimal energy to displace the PKA from its lattice site, which corresponds to the threshold energy to initiate a replacement sequence. For the other two directions, E_d values are determined using the standard definition when a stable Frenkel pair is created based on the Wigner-Seitz defect analysis.

In general, the values of E_d determined for pure Ni compare well with available experimental values, which are 38 eV, 21 eV and 60 eV along the [100], [110] and [111] directions, respectively [31]. Note that previous MD simulations yielded values of 32 eV, 38 eV and 58 eV in these three directions, respectively [13]. Compared to previous AIMD results in pure Ni calculated at 0 K [24], it is suggested from Fig. 2 that including an initial temperature distribution does not induce substantial differences in the values of E_d. In our calculations, different PKAs result in different values of E_d at finite temperature due to random arrangement of elements and associated thermal fluctuations. There are noticeable differences in the calculated E_d values for Ni and Co along the [100] direction compared to the results calculated in ordered NiCo [24]. The differences may arise from the difference in disordered and ordered structures. In ordered structures, Ni (Co) only collides with Ni(Co), whereas atom collisions are randomized in this study.

Comparing the values of E_d in these three systems, the E_d values in NiCo are similar or even slight higher than those in pure Ni for all three directions considered. However, the E_d values in NiFe show some distinct features. While the E_d values along the [100] and [110] directions are similar to those found in NiCo and Ni, lower E_d values are observed in the [111] direction for Fe recoils in NiFe. To verify the difference in the values of E_d for Ni and Fe in the [111] direction, two additional simulations were performed. The results are also given in Fig. 2, which suggest that the E_d values of Fe in NiFe are indeed lower than those of Ni and Co along the [111] direction in Ni and NiCo.

To differentiate the role of chemical and displacement fluctuation disorder, the atomic trajectories involved in the collision cascade are analyzed in detail. The results are given in the Supplementary Information. It is found that there are no noticeable differences for atomic trajectories in NiFe compared to those in pure Ni and NiCo. This observation suggests that the site-to-site distortions have little effect on the values of E_d. As shown in Fig. 1, Ni and Fe atoms experience larger radial displacement in NiFe compared to NiCo and Ni. However, the atomic trajectories in these three systems are very similar.

The calculated E_d has taken into account the effect of thermal fluctuations and intrinsic chemical disorder in CSAs. To clarify their different roles, the E_d values in Ni, NiCo and NiFe along the [111] direction are compared to the results calculated using the same PKA in a static perfect lattice without thermal fluctuations. In such a lattice, the effect of displacement fluctuations is minimized. The E_d values obtained, as well as the trajectories of those atoms involved in the low-energy recoil events, are provided in Fig. 3. The comparison indicates that the displacement disorder in Ni does not induce significant change to E_d in Ni; whereas a large variation in E_d is found in NiCo and NiFe due to displacement fluctuations. The variation is opposite in NiCo and NiFe, suggesting the random nature of the disorder. In the perfect lattice, a PKA with an energy of E_d in the close-packed A plane passes through the two triangular centers in the first and second nearest {111} planes (B and C planes), and then directly collides with an atom in the third neighboring A plane. In pure Ni, the Ni PKA scatters off the three atoms in the B and C planes symmetrically and symmetric trajectories are ob-

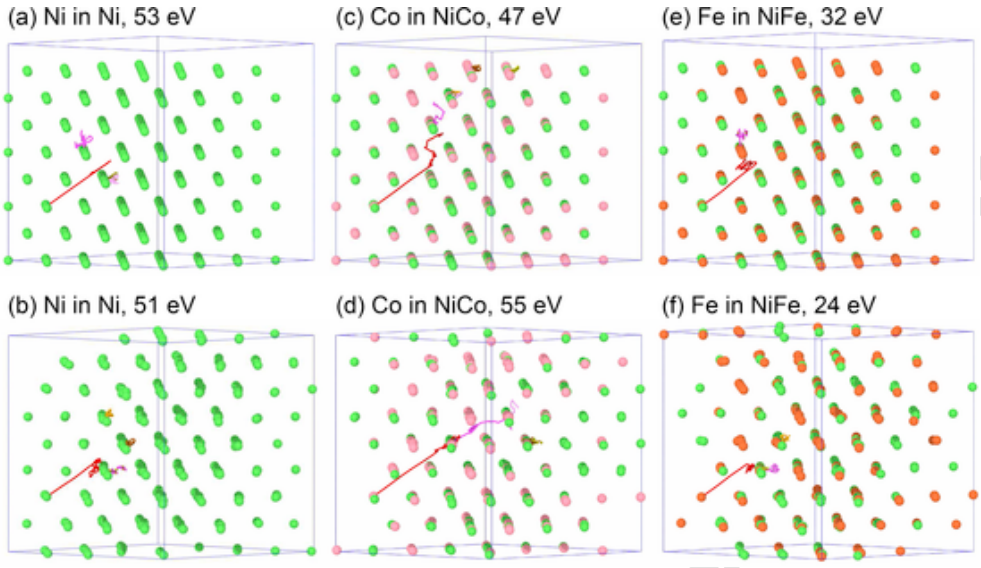

Fig. 3. The trajectories of those atoms experiencing significant displacement during the low-energy recoil events along the [111] direction as well as the determined E_d. The upper row shows results simulated in static perfect *fcc* lattices, whereas results in the lower row include initial thermal fluctuations. Ni atoms are denoted by green balls, while Co and Fe atoms are represented by pink and orange balls. The trajectories of different atoms are denoted by lines with different colors. (For interpretation of the references to color in this figure legend, the reader is referred to the Web version of this article.)

served (Fig. 3(a)) The PKA finally creates an interstitial at an octahedral site and leaves a vacancy at its original location. Including the thermal fluctuations change the trajectories of the atoms in the recoil region and makes the interstitials more likely to be in the form of [100] dumbbells. In NiCo and NiFe, the atomic trajectories are strongly dependent on the local environment. Note that lower E_d values are always found in NiFe for Fe recoils, no matter whether the initial relaxations are included or not. Thus, it is the property of a specific element that plays a decisive role in governing the E_d values.

3.1.2. Defect structures

The atomic configurations following the recoil events provide information on the properties of resulting defects. As discussed above, recoils along the [110] direction induce a long replacement collision sequence. Therefore, the created defect structure is basically a chain of atomic replacements. In pure Ni, the last recoil atom occupies the vacancy left by the PKA and no defect is seen by the Wigner-Seitz defect analysis. In NiCo and NiFe, the atomic replacement generates lots of antisite defects since one atom may occupy the lattice location of another atom belonging to different atom types.

For recoils along the [100] and [111] directions, the resulting defects are Frenkel pairs. While a vacancy is produced by the displaced PKA, the interstitial structure is dependent on the recoil directions, as well as the local atomic environment. It is known that the most stable interstitial configuration in *fcc* Ni at 0 K is the [100] dumbbell, in which two atoms align along the [100] direction sharing the same lattice site [15,32]. We have analyzed the defect structure produced in this work. For this purpose, the orientation of the dumbbell axis in the final state is calculated with respect to the closest [100] direction and the deviation angle (θ) is obtained. The results are summarized in Table 1, together with the dumbbell compositions, the distance between the two atoms inside the dumbbell (d_{dumbbell}), and the distance between the vacancy and interstitial inside the Frenkel pair ($d_{\mathrm{V\text{-}I}}$) determined by Wigner-Seitz defect analysis.

The results in Table 1 show that most deviation angles are smaller than 16°, indicating that [100] dumbbells are energy preferred configurations in low-energy recoil events. Nevertheless, large deviations are observed in some cases, and a [111] dumbbell is found in NiCo. These deviations can be attributed to alloying effects and thermal fluctuations. In fact, *ab initio* calculations at 0 K suggest the axis of dumbbells in CSAs is not strictly along the lattice direction because of the disorder [15]. Previous calculations also suggest that the defect energies in CSAs exhibit distributions [15]. Therefore, the appearance of [111] dumbbells does not necessarily imply an energy preference of [111] dumbbells over [100] dumbbells. It is highly likely that the distributions of their formation energies have some overlap regions. The distance between the two atoms in the dumbbell structure is around 2 Å in all cases, as shown in Table 1, similar to that found in static calculations [15].

For the recoils in the [100] direction, the PKAs rarely form dumbbells. In this case, most of the PKA are displaced from their original lattice site and occupy another site, as can be seen from the atomic trajectories in the Supplementary Information. Instead, the final dumbbell defect is created by the secondary recoil atom and even the third recoil atom. In random alloys, it is possible that the PKA replaces another lattice atom with a different atom type, thus resulting in antisite defects besides the Frenkel pair defect. In contrast, in the [111] direction, most of the dumbbells produced contains the PKA atom. In this case, the PKA loses most of its kinetic energy when it passes through the close-packed planes. As a result, there is enough time for the PKA to interact with other lattice atoms to create dumbbell defects.

The separation distance between the vacancy and interstitial comprising a Frenkel pair ranges from 4 to 10 Å, which reflects the extent to which the low-energy recoil event will have disturbance on the lattice structure. The differences from three independent PKAs are small in pure Ni, whereas much larger differences are observed in CSAs. This can be attributed to the disorder inherent in CSAs.

3.2. $Ni_{0.8}X_{0.2}$ (X = Fe, Co, Cr, Pd) CSAs

To further compare alloying effects of different elements in terms of *d* electron number, atomic volume and mass, the values of E_d in four $Ni_{0.8}X_{0.2}$ (X = Fe, Co, Cr, Pd) CSAs along the [111] direction are calculated. This direction is chosen because E_d values show the most visible differences in this direction as found in equiatomic NiCo and NiFe. Since the above results suggest that the effects of initial thermal fluctuation on E_d values are limited, the initial temperature is set to be 0 K in these AIMD calculations. The obtained results for Ni and X atoms

Table 1
Defect configurations determined in low energy recoil events when the recoil energy is E_d. The dumbbell orientations (θ) are measured with respect to the [100] direction, unless otherwise indicated. The dumbbell composition, the distance between the two atoms in the dumbbell structure (d_{dumbbell}) and the distance between the vacancy and interstitial in the Frenkel pair ($d_{\text{V-I}}$) determined by Wigner-Seitz defect analysis are also provided. All distances are given in angstrom. The dumbbells formed by the PKA are denoted by superscript.

	[100] PKA				[111] PKA			
	θ	Composition	d_{dumbbell}	$d_{\text{V-I}}$	θ	Composition	d_{dumbbell}	$d_{\text{V-I}}$
Ni	2.58°	[010]Ni–Ni	2.12	6.59	3.97°	[100]Ni–Ni	2.10	4.32
	15.43°	[010]Ni–Ni	2.10	7.05	18.11°	[100]Ni ^{PKA}-Ni	2.23	4.36
	15.45°	[001]Ni–Ni	2.00	5.57	12.30°	[010]Ni ^{PKA}-Ni	2.08	6.14
Ni in NiCo	17.15°	[100]Co–Co	2.14	7.87	4.93°	[001]Co–Co	2.23	4.31
	12.18°	[001]Ni–Ni	2.00	7.05	12.24°	[010]Ni ^{PKA}-Co	2.02	8.22
	9.59°	[100]Ni ^{PKA}-Co	2.28	5.57	9.88°	[001]Ni ^{PKA}-Ni	2.12	4.24
Co in NiCo	13.95°	[010]Ni–Co	2.08	11.14	4.39° [a]	[111]Co–Co	2.11	6.09
	10.23°	[100]Ni–Ni	2.19	10.27	11.73°	[100]Ni–Co	2.28	5.52
	15.06°	[010]Co–Co	1.86	10.57	15.04°	[100]Co ^{PKA}-Ni	1.95	6.63
Ni in NiFe	5.20°	[100]Ni–Fe	1.99	10.27	17.87°	[100]Ni–Fe	2.14	9.14
	3.58°	[100]Ni ^{PKA}-Ni	2.00	3.52	9.92°	[100]Ni–Fe	2.20	5.60
	9.26°	[010]Fe–Fe	1.93	5.57	6.11°	[001]Ni–Ni	2.03	5.52
Fe in NiFe	7.16°	[100]Ni–Fe	2.17	10.27	5.56°	[100]Fe ^{PKA}-Fe	2.05	4.33
	10.62°	[010]Fe ^{PKA}-Ni	2.09	5.57	3.23°	[100]Fe–Fe	1.95	8.22
	13.68°	[001]Fe–Fe	1.90	5.57	3.41°	[100]Fe–Fe	2.05	6.53

[a] [111] dumbbell. θ is calculated with respect to the [111] direction.

are presented in Fig. 4. To verify the trend of E_d values, three and five independent calculations are performed for Ni and X in each alloy, respectively. It is suggested that the E_d values of Ni and X in $Ni_{0.8}Fe_{0.2}$, $Ni_{0.8}Co_{0.2}$ and $Ni_{0.8}Cr_{0.2}$ are similar, both ranging from 47 to 62 eV. In $Ni_{0.8}Pd_{0.2}$, the E_d values of Ni are higher (in the range of 60–70 eV), whereas those of Pd are lower (less than 45 eV). The difference in $Ni_{0.8}Pd_{0.2}$ can be attributed to mass effects, since Pd is much heavier than Ni. As a result, less energy is required for Pd to create stable defects in the lattice. For $Ni_{0.8}Fe_{0.2}$, $Ni_{0.8}Co_{0.2}$ and $Ni_{0.8}Cr_{0.2}$, their similar E_d values suggest alloying effects are limited regarding to threshold energies.

4. Discussion

The primary goal of present study is to investigate the effects of chemical disorder on low-energy recoil events in CSAs. The results show that the most significant influence on E_d values are Fe recoils along the [111] direction. To gain insight into this observation, additional simulations were performed by playing with local atomic environments around a Fe PKA inside a pure Ni matrix. The initial atomic configurations, calculated E_d values and associated defect structures are presented in Table 2.

Table 2 shows that the E_d value of a single Fe atom inside Ni is 55 eV. This value is similar to that of Ni in Ni (53 eV) as displayed in Fig. 3. A sudden decrease of E_d value from 55 to 44 eV is found when the atoms in the nearest close-packed plane along the [111] path are replaced by Fe atoms, whereas the E_d value remains around 50 eV when Fe appears in the second nearest close-packed plane. Further decrease is observed when all three atoms are Fe in the first nearest close-placed plane. This result suggests interactions among Fe PKA and other Fe atoms along the recoil path help to lower E_d values. Further insight can be gained from the analysis of PKA trajectories. Here the PKA trajectory of a Fe PKA with an energy of 44 eV is presented in Fig. 5 when an atom in the nearest {111} plane is replaced by Fe. It shows that the PKA first passes through the first triangle but fails to pass the second one. At 0.3 ps, the PKA bounces back towards the vacancy left behind. In this process, the PKA loses most of its kinetic energy. The bounced Fe PKA could pass through the triangle and recombine with the vacancy if there is no Fe atom in the first triangle, as indicated by the high E_d value of 55 eV. However, in the case shown in Fig. 5, the Fe PKA cannot go back to the vacancy position, possibly due to repulsive interactions between Fe–Fe atoms. This repulsive interaction has been previously reported from DFT calculated binding energies [32]. The repulsive interaction is in accordance with the higher formation energies of Fe–Fe dumbbells in Ni–Fe alloys [8,15,33]. Consequently, the PKA is trapped between the two nearest {111} planes and finally forms a dumbbell with a Ni atom. Therefore, the low E_d value found in Fe PKA is a result of the peculiar interaction between Fe–Fe atoms.

To confirm that the electron configuration of an alloying element plays a significant role in energy transfer (e.g. a Fe atom is difficult to pass through the nearest {111} planes) as shown in Fig. 5, additional NEB calculations are performed to study the energy barrier for this process. The results are shown in Fig. 6. For comparison, the results for Co and Cr are also provided. Here the initial state is a [010] Fe (Co, Cr)–Ni dumbbell created by the PKA and the vacancy left, which corresponds to a Frenkel pair defect. The energy of this defect is around 5.49, 5.34 and 5.13 eV higher in Fe, Co and Cr cases respectively, compared to those of final states where all atoms are in lattice positions. It is found that the energy barrier for Fe to recombine with the vacancy is about 0.50 eV, whereas it is 0.21 and 0.18 eV for Co and Cr, respectively. The energy barrier of 0.50 eV is much higher compared to the migration barrier of a Fe–Ni interstitial dumbbell in the Ni matrix (0.11 eV [32]). Therefore, the produced Fe–Ni interstitial dumbbell prefers to migrate in the matrix rather recombines with the vacancy. In contrast, the barriers are lower for Co and Cr, which indicate that recombination is easier in Co and Cr cases. To understand this distinct behavior, the projected electronic densities of states (PDOS) for Fe,

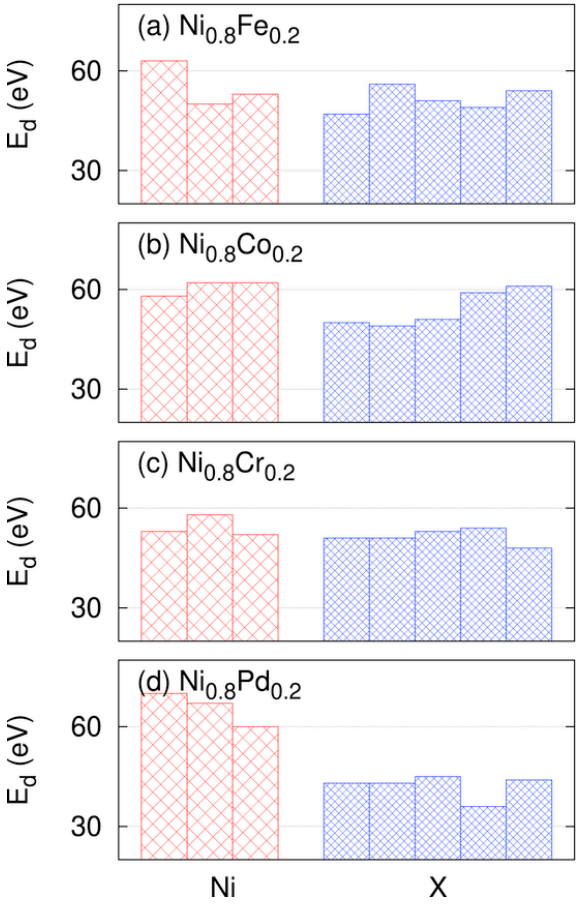

Fig. 4. Threshold displacement energy in $Ni_{0.8}X_{0.2}$ (X = Fe, Co, Cr, Pd) CSAs along the [111] direction.

Table 2
Threshold displacement energy of Fe in Ni matrix under different local atomic environments.

E_d (eV)	Defect structure	Atomic arrangement
55	[001]Fe ^{PKA}-Ni	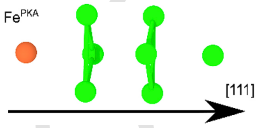
44	[001]Fe ^{PKA}-Ni	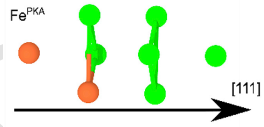
52	[001]Fe ^{PKA}-Fe	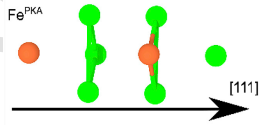
25	[001]Fe ^{PKA}-Ni	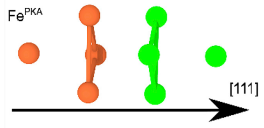
26	[001]Fe ^{PKA}-Fe	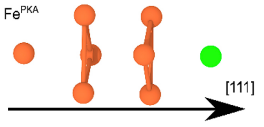
23	[010]Fe ^{PKA}-Fe	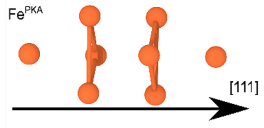

Co and Cr PKA are also given in Fig. 6. For Fe PKA, the DOS at Fermi level is much higher at the saddle configuration compared to that at the initial state. Therefore, the corresponding band energy in the saddle is higher than that in the initial configuration, which results in high energy barrier for Fe. On the other hand, the DOS for Co and Cr PKA are only slightly changed from the initial state to saddle configuration, in agreement with the low values of energy barrier. The difference in PDOS of Fe and Co can be understood within rigid band approximation and is attributed to electron occupation changes. Since Co has one more electron than Fe, the Fermi level should be shifted to higher energy, relative to its position in Fe, to accommodate the additional electron. As a result, the PDOS in the spin-up channel near Fermi level becomes flat in Co compared to Fe. The lower E_d values of Fe in NiFe along the [111] direction suggest that it is easier to create stable defects in this direction. As a result, the damage induced by ion irradiation in NiFe should be more delocalized and scattered, since local recombination is less probable.

The results above demonstrate that the presence of Fe in the nearest {111} planes can further decreases E_d values, whereas Co and Cr presence in the same location have little effects. To better understand the difference, the energy profile is calculated when the PKA moves from its original location along the [111] direction. The results for Fe, Co and Cr in different chemical environments are shown in Fig. 7. In these calculations, the atomic positions are fixed. Along this path, the PKA goes through two triangular centers in the nearest {111} planes, as evident by the two peaks in energy curves. The gray area represents the energy profile for a Ni in a Ni matrix. Fig. 7 show that an increase of Fe atom concentration in the nearest {111} plane causes significant decrease of energy in the first peak (~4 eV), whereas only limited effect is observed in the cases of Co or Cr. This reduction of first peak value suggests that less energy is required for the Fe PKA to pass through the first triangle center and create stable defects, thus decreas-

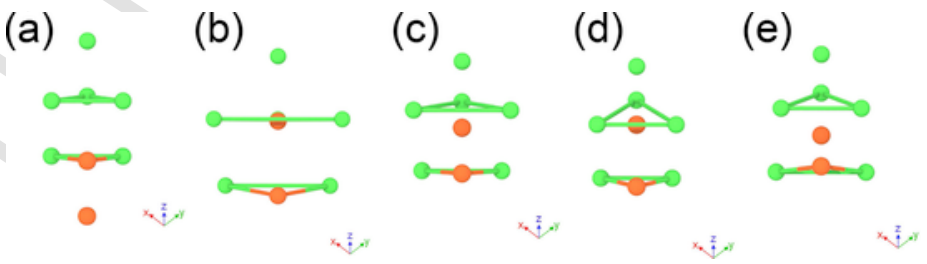

Fig. 5. A Fe PKA trajectory at energy of E_d (44 eV). (a) 0 ps, (b) 0.1 ps, (c) 0.3 ps, (d) 0.8 ps and (e) 1.0 ps.

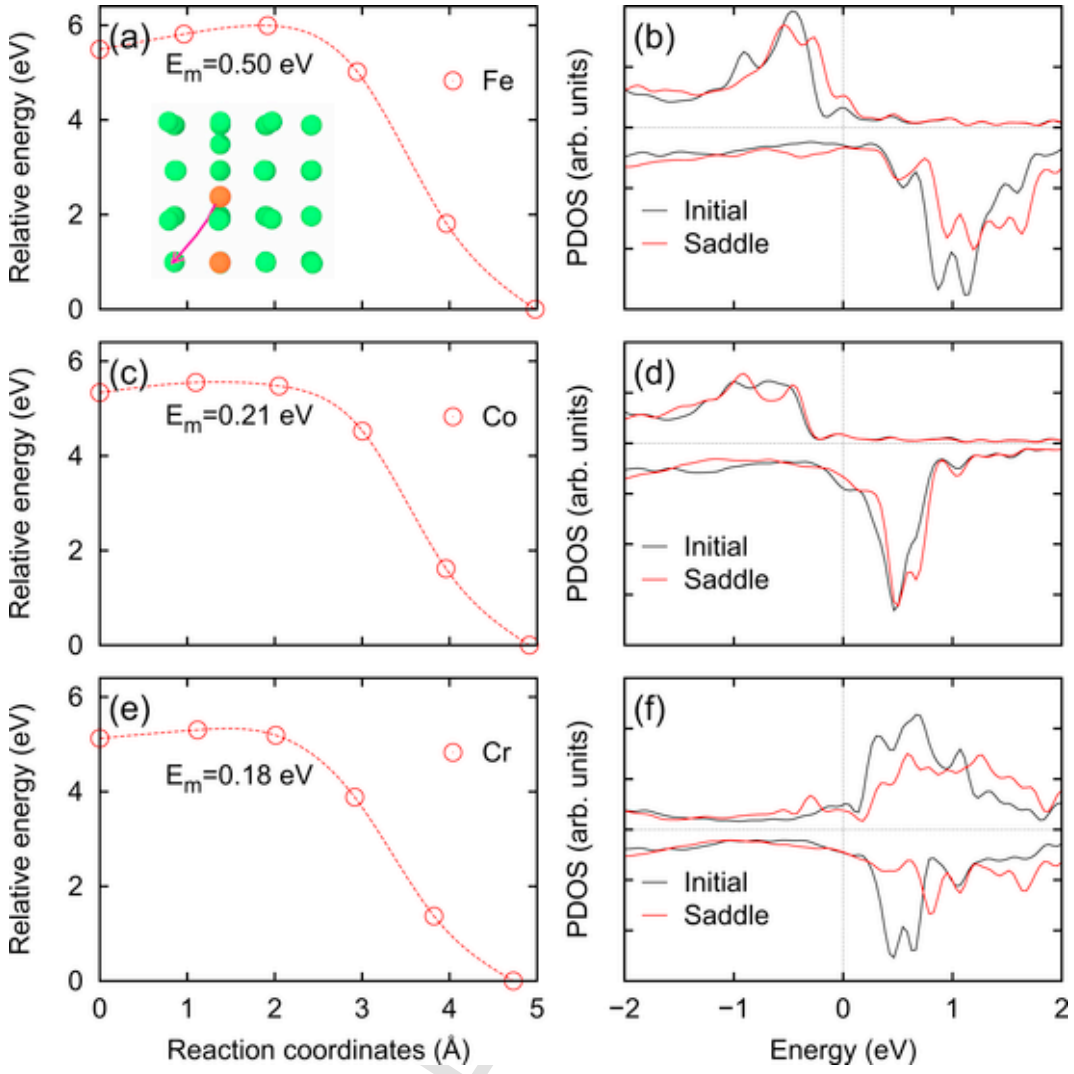

Fig. 6. Energy profile of recombination between a [010] interstitial dumbbell and a vacancy produced by a PKA in Ni–Fe, Ni–Co and Ni–Cr. E_m is the migration energy defined as the energy difference between the maximal energy and the initial energy. In the right column, the corresponding PDOS of the PKA is shown in the initial and saddle configurations. The Fermi level is set to be 0 eV.

ing E_d values. For Co and Cr, their energy profiles are similar to that of Ni in a Ni matrix, which are consistent with their similar E_d values. These differences can be traced back to their differences in electronic structure, as provided by PDOS when the PKA is located in the center of the first triangle. In this configuration, the magnetic moment of PKA is suppressed because of volume compression, which results in smaller differences between spin-up and spin-down channels as Fe (Co, Cr) concentration increases. Accordingly, the DOS peak in the left of the Fermi level gradually shifts to higher energies with increasing Fe (Co, Cr), which leads to a reduction of band energy. At 0 K, band energy can be written as $E_b = \int_{-\infty}^{E_F} (E - E_F) f(E)\, dE$, where E_F is the Fermi level and $f(E)$ is electronic DOS. Only the electronic DOS below the Fermi level (occupied states) contributes to band energy. In the case of Fe, the occupied states decrease rapidly with increasing Fe (Fig. 7(b)), consistent with the large drop of energy observed in Fig. 7(a). The change of occupied states in Co is smaller than Fe, so is the calculated energy in Fig. 7(c). For Cr, the DOS is almost flat near Fermi level, which results in small energy difference in Fig. 7(e). Therefore, the energy change can be explained by band filling effects. Among these three elements, increasing Cr has little effect on energy profiles, and thus its effect on E_d values is limited.

In our calculations, we have distinguished two kinds of disorder in the CSAs, one is the lattice distortion effects, and the other is the random elemental arrangement. Our results indicate that the chemical disorder in NiCo does not have a significant influence on the threshold energies in both [100] and [111] directions. On the other hand, chemical disorder indeed has a remarkable impact on threshold energies in NiFe, particularly along the [111] directions. Our analysis further illustrates that the electronic structure of elements plays a crucial role in affecting the defect creation mechanism. Therefore, the chemical disorder can affect defect production in CSAs through complexed interactions at the electronic level.

5. Conclusion

AIMD simulations have been performed to study low-energy recoil events in Ni, $Ni_{50}X_{50}$ (X = Fe and Co), and $Ni_{80}X_{20}$ (X = Fe, Co, Cr and Pd) disordered CSAs. The chemical disorder is considered by SQS structures and the inherent atomic displacements are included by initial MD runs. Anisotropic E_d values in these materials are demonstrated. Specifically, the highest E_d values are observed along the [111] direction. On the other hand, the recoil events along the [110] direction produces a replacement collision sequence, and the minimal energy required for initializing such sequence is low. Among the PKA direc-

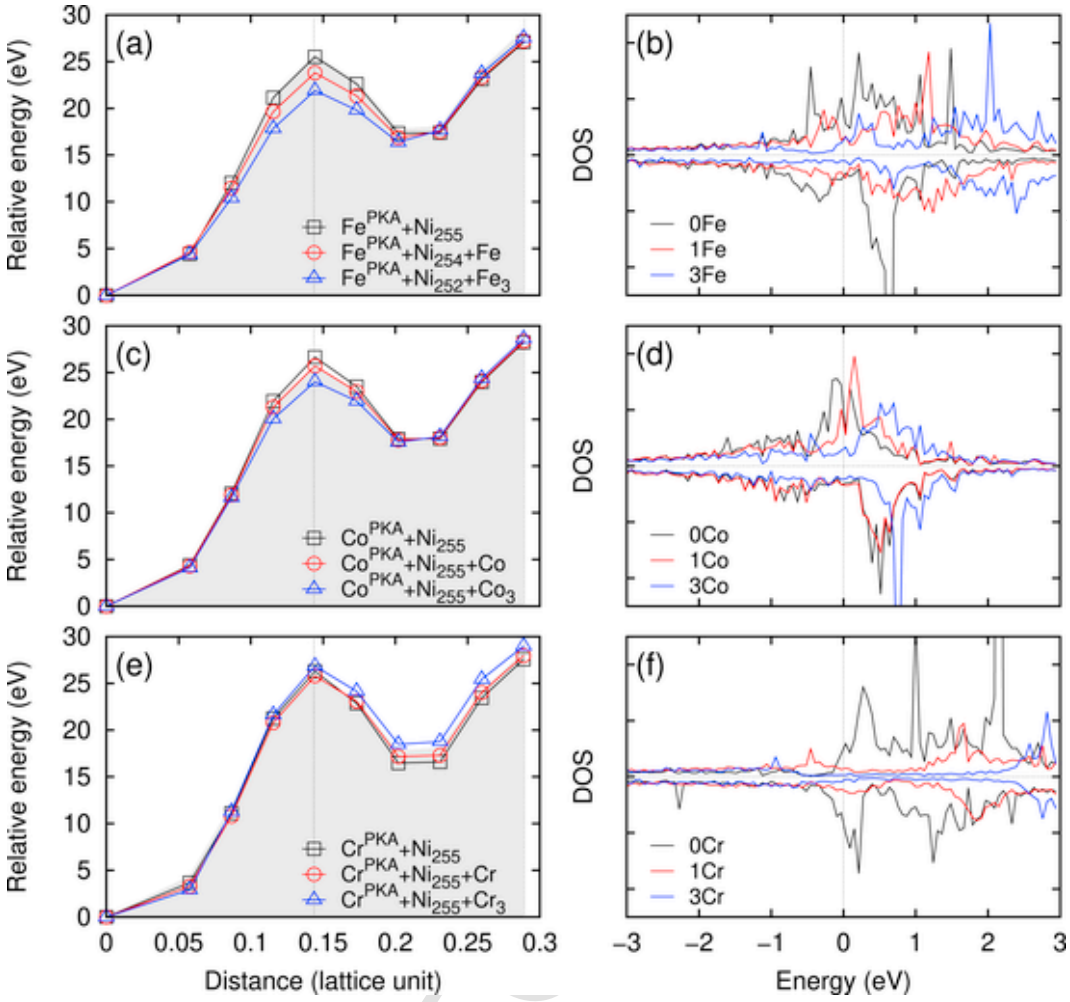

Fig. 7. Energy profile when a Fe, Co and Cr PKA move along the [111] direction in different local chemical environment. The gray area represents the energy profile for a Ni in a Ni matrix. Three cases are shown: Fe (Co, Cr) PKA in Ni matrix, Fe (Co, Cr) PKA in Ni matrix in which one Ni atom in the nearest {111} plane is replaced by Fe (Co, Cr), and Fe (Co, Cr) PKA in Ni matrix in which three Ni atoms in the nearest neighbor {111} plane are replaced by Fe (Co, Cr). The two dashed lines denote triangular center in the two nearest {111} planes. In the right column, the calculated PDOS of *d* states are shown when the PKA is located at the first center of the nearest {111} plane. The Fermi level is set to be 0 eV.

tions studied, the calculated values of E_d for Fe in NiFe along the [111] direction is lower than that in Ni and NiCo. Our analysis further shows that chemical disorder due to random arrangement of different elements has a larger effect than thermal displacement on E_d values. In particular, Fe atoms tend to lower E_d values in the [111] direction, compared to Co and Cr. The present results underline the importance of chemical disorder in determining the defect production in CSAs.

CRediT authorship contribution statement

Shijun Zhao: Methodology, Data curation, Writing - original draft. **Bin Liu:** Writing - review editing. **German D. Samolyuk:** Methodology, Writing - review editing. **Yanwen Zhang:** Writing - review editing. **William J. Weber:** Writing - review editing.

Declaration of competing interest

The authors declare no conflict of interests.

Acknowledgment

This work was supported as part of the Energy Dissipation to Defect Evolution (EDDE), an Energy Frontier Research Center funded by the U.S. Department of Energy, Office of Science, Basic Energy Sciences.

Appendix A. Supplementary data

Supplementary data to this article can be found online at https://doi.org/10.1016/j.jnucmat.2019.151941.

References

[1] B. Gludovatz, A. Hohenwarter, D. Catoor, E.H. Chang, E.P. George, R.O. Ritchie, A fracture-resistant high-entropy alloy for cryogenic applications, Science 345 (2014) 1153–1158.
[2] M.-H. Tsai, J.-W. Yeh, High-entropy alloys: a critical review, Mater. Res. Lett. 2 (2014) 107–123.
[3] D.B. Miracle, O.N. Senkov, A critical review of high entropy alloys and related concepts, Acta Mater. 122 (2017) 448–511.
[4] Y. Zhang, S. Zhao, W.J. Weber, K. Nordlund, F. Granberg, F. Djurabekova, F. Granbergc, F. Djurabekova, Atomic-level heterogeneity and defect dynamics in concentrated solid-solution alloys, Curr. Opin. Solid State Mater. Sci. 21 (2017) 221–237.
[5] Y. Zhang, G.M. Stocks, K. Jin, C. Lu, H. Bei, B.C. Sales, L. Wang, L.K. Béland, R.E. Stoller, G.D. Samolyuk, M. Caro, A. Caro, W.J. Weber, Influence of chemical disorder on energy dissipation and defect evolution in concentrated solid solution alloys, Nat. Commun. 6 (2015) 8736.
[6] Y. Zhang, K. Jin, H. Xue, C. Lu, R.J. Olsen, L.K. Beland, M.W. Ullah, S. Zhao, H. Bei, D.S. Aidhy, G.D. Samolyuk, L. Wang, M. Caro, A. Caro, G.M. Stocks, B.C. Larson, I.M. Robertson, A.A. Correa, W.J. Weber, Influence of chemical disorder on energy dissipation and defect evolution in advanced alloys, J. Mater. Res. 31 (2016) 2363–2375.
[7] S. Zhao, G. Velisa, H. Xue, H. Bei, W.J. Weber, Y. Zhang, Suppression of vacancy cluster growth in concentrated solid solution alloys, Acta Mater. 125 (2017) 231–237.

[8] S. Zhao, W.J. Weber, Y. Zhang, Unique challenges for modeling defect dynamics in concentrated solid-solution alloys, JOM (J. Occup. Med.) 69 (2017) 2084–2091.
[9] Y.N. Osetsky, L.K. Béland, R.E. Stoller, Specific features of defect and mass transport in concentrated fcc alloys, Acta Mater. 115 (2016) 364–371.
[10] F. Granberg, K. Nordlund, M.W. Ullah, K. Jin, C. Lu, H. Bei, L.M. Wang, F. Djurabekova, W.J. Weber, Y. Zhang, Mechanism of radiation damage reduction in equiatomic multicomponent single phase alloys, Phys. Rev. Lett. 116 (2016) 135504.
[11] S.I. Golubov, A.V. Barashev, R.E. Stoller, Radiation damage theory, in: R.J.M. Konings, Comprehensive Nuclear Materials, 1, Elsevier, Amsterdam, 2012, pp. 357–391 (n.d).
[12] M. Norgett, M. Robinson, I. Torrens, A proposed method of calculating displacement dose rates, Nucl. Eng. Des. (1975).
[13] F. Gao, D.J. Bacon, Point-defect and threshold displacement energies in Ni_3Al II. Events at the displacement threshold, Philos. Mag. A 67 (1993) 289–306.
[14] C. Dimitrov, B. Sitaud, O. Dimitrov, Displacement threshold energies in Ni(Al) solid solutions and in Ni3Al, J. Nucl. Mater. 208 (1994) 53–60.
[15] S. Zhao, G.M. Stocks, Y. Zhang, Defect energetics of concentrated solid-solution alloys from ab initio calculations: $Ni_{0.5}Co_{0.5}$, $Ni_{0.5}Fe_{0.5}$, $Ni_{0.5}Fe_{0.5}$ and $Ni_{0.5}Cr_{0.5}$, Phys. Chem. Chem. Phys. 18 (2016) 24043–24056.
[16] L.K. Béland, C. Lu, Y.N. Osetskiy, G.D. Samolyuk, A. Caro, L. Wang, R.E. Stoller, Features of primary damage by high energy displacement cascades in concentrated Ni-based alloys, J. Appl. Phys. 119 (2016) 085901.
[17] H.Y. Xiao, W.J. Weber, Y. Zhang, X.T. Zu, Ab initio molecular dynamics simulations of ion–solid interactions in zirconate pyrochlores, Acta Mater. 87 (2015) 273–282.
[18] H.Y. Xiao, W.J. Weber, Y. Zhang, X.T. Zu, S. Li, Electronic excitation induced amorphization in titanate pyrochlores: an ab initio molecular dynamics study, Sci. Rep. 5 (2015) 8265.
[19] G. Kresse, J. Furthmüller, Efficiency of ab-initio total energy calculations for metals and semiconductors using a plane-wave basis set, Comput. Mater. Sci. 6 (1996) 15–50.
[20] P.E. Blöchl, Projector augmented-wave method, Phys. Rev. B. 50 (1994) 17953.
[21] J.P. Perdew, K. Burke, M. Ernzerhof, Generalized gradient approximation made simple, Phys. Rev. Lett. 77 (1996) 3865.
[22] J.M. Cowley, Short-range order and long-range order parameters, Phys. Rev. 138 (1965) A1384.
[23] J.M. Cowley, An approximate theory of order in alloys, Phys. Rev. 77 (1950) 669.
[24] B. Liu, F. Yuan, K. Jin, Y. Zhang, W.J. Weber, Ab initio molecular dynamics investigations of low-energy recoil events in Ni and NiCo, J. Phys. Condens. Matter 27 (2015) 435006.
[25] W.G. Hoover, Canonical dynamics: equilibrium phase-space distributions, Phys. Rev. A 31 (1985) 1695.
[26] S. Nosé, A unified formulation of the constant temperature molecular dynamics methods, J. Chem. Phys. 81 (1984) 511–519.
[27] P. Olsson, C.S. Becquart, C. Domain, *Ab initio* threshold displacement energies in iron, Mater. Res. Lett. 4 (2016) 219–225.
[28] S. Zhao, J. Xue, C. Lan, L. Sun, S. Yan, Influence of high pressure on the threshold displacement energies in silicon carbide: a Car–Parrinello molecular dynamics approach, Nucl. Instrum. Methods Phys. Res. Sect. B Beam Interact. Mater. Atoms 286 (2012) 119–123.
[29] F. Gao, H. Xiao, X. Zu, M. Posselt, W.J. Weber, Defect-enhanced charge transfer by ion-solid interactions in SiC using large-scale *Ab initio* molecular dynamics simulations, Phys. Rev. Lett. 103 (2009) 027405.
[30] G. Bonny, N. Castin, D. Terentyev, Interatomic potential for studying ageing under irradiation in stainless steels: the FeNiCr model alloy, Model. Simul. Mater. Sci. Eng. 21 (2013) 85004.
[31] A. Bourret, Irradiation damage in nickel and iron in a high-voltage electron microscope and threshold energy determination, Phys. Status Solidi 4 (1971) 813–825.
[32] J.D. Tucker, T.R. Allen, D. Morgan, Ab initio defect properties for modeling radiation-induced segregation in Fe-Ni-Cr alloys, 13th Environ. Degrad. Mater. Nucl. Power Syst. (2007).
[33] S. Zhao, Y. Osetsky, Y. Zhang, Preferential diffusion in concentrated solid solution alloys: NiFe, NiCo and NiCoCr, Acta Mater. 128 (2017) 391–399.